UCLA

THE EFFECTS OF PROCESSING AND CONSTITUENT MATERIALS ON COMPRESSIVE STRENGTH OF THICK COMPOSITE LAMINATES

AD-A271 912

H. T. HAHN
E. A. KEMPNER
J. SLAUGHTER

ANNUAL REPORT
AUGUST, 1993

DTIC

NOV 01 1993

D

Approved for public release
Distribution

Mechanical, Aerospace and Nuclear Engineering Dept.
Engineering IV
UCLA
Los Angeles, CA 90024-1597
Tel: 310 825 2383
Fax: 310 206 2302

93-26049

93 10 27 003

I. OBJECTIVES

The objectives of this study pertain to both the processing of thick composites and the constituent materials used. The main objectives of the research are to identify the processing conditions that are responsible for fiber wrinkling in thick, filament-wound cylinders and to develop a process simulation model for filament winding of thick cylinders. Analysis-experiment correlation will be used to aid model development. Also, the effect of constituent materials on compressive strength will be studied. This will be accomplished by identifying the fiber microstructure responsible for low compressive strength and developing an analytical model relating fiber microstructure to compressive strength.

II. PROGRESS

The focus of the research during the first year has been primarily on experimentally and analytically determining the processing conditions responsible for fiber wrinkling in thick filament-wound cylinders. An experimental study has been undertaken to investigate the effect of various processing conditions on the final quality of thick cylinders. Meanwhile, a process simulation model has been developed in conjunction with the experimental results. The simulation model will be applied to all stages of the filament winding process and will be evaluated with experimental correlation.

One paper has been published based on the analytical model development for this project. "The Effect of Radial Stress Relaxation on Fiber Stresses in Thick Filament-Wound Cylinders" was presented at the 1993 International Conference on Composite Materials [1]. In this paper, the stress redistribution due to fiber motion in thick, filament-wound cylinders was analyzed. It was concluded that an increased probability of fiber buckling exists due to stress relaxation after winding thick cylinders. A copy of the manuscript is enclosed.

A. Analytical Model Development

Analytical models have been developed to describe most problems in the filament winding process. Winding models have been developed based on elastic analyses for composite winding as well as for materials used in other industries [2-4]. Complete process models were developed that include the effect of resin flow, heat transfer and cure kinetics throughout the process [5-7]. Special features observed during filament winding of composite structures were detailed by Tarnopol'skii and Beil' [8]. They pointed out the nonlinear anisotropy evident during filament winding due to the compressibility of the cylinder in the radial direction. To investigate the effect of the nonlinear compressibility in the radial direction they developed winding models based on linear, piecewise linear and nonlinear elastic analyses. Gutowski, et al. explained the nonlinear transverse compressibility of fiber tows by pointing out the essential waviness and misalignments of fibers within a bundle [9-10].

Based on existing analyses, it was concluded that a significant contribution could be made by developing a model for the compaction of a fiber network and incorporating

the model for compaction with resin flow and residual stress models to develop one unified analytical model.

A. 1. Fiber Compaction

Consider a fiber preform consisting of many fibers stacked and bundled. Although the fibers are oriented, the massive number of fibers makes perfect alignment impossible. Therefore, the fibers contact each other at discrete points. Assume the fibers are composed of a linear elastic material. As the preform is compacted transverse to the fibers, deformation occurs due to the straightening of the fibers rather than compression of the fibers themselves. The bending of the fibers is assumed to behave like the bending of a beam. The low resistance of the fibers to bending results in a very low compressive modulus. Also, as discussed in [8], the resulting deformation is actually nonlinear.

To characterize the fiber network, a simple, two dimensional representative volume element is used. The shape of each fiber is approximated by a sine wave as shown in Figure 1. The initial fiber shape is given by the equation

$$y = \frac{a}{2}\cos\frac{\pi x}{L/2} \tag{1}$$

where a is the fiber amplitude and L is the fiber wavelength. Assuming the fibers are spaced side by side at a distance d, the initial fiber volume fraction, V_{fo}, is given by

$$V_{fo} = \frac{\pi d_f^2}{4(a+d_f)d} \tag{2}$$

where d_f represents the fiber diameter. Rearranging, the ratio between fiber spacing and fiber diameter is found.

$$\frac{d}{d_f} = \frac{\pi}{4}\frac{1}{(a/d_f+1)}\frac{1}{V_{f0}} \tag{3}$$

Equating the fiber volume before and after compaction yields the equation

$$V_{f\max}d_f d = V_{fo}(a+d_f)d \tag{4}$$

where $V_{f\max}$ is the fiber volume fraction after maximum compaction. Rearranging, the ratio between fiber wave amplitude and fiber diameter can also be found.

$$\frac{a}{d_f} = \frac{V_{f\max}}{V_{f0}} - 1 \tag{5}$$

2

Figure 2 shows the fiber as it is being deformed. Assuming the fibers contact at the peaks of each wave, compaction will flatten these peaks. The deformation of the peaks is denoted by Δy and half the length of the deformed portion is Δx. The deformed fiber shape is given by

$$\frac{a}{2} - \Delta y = \frac{a}{2}\cos\left(\frac{\pi\Delta x}{L/2}\right) \tag{6}$$

The length of the undeformed fiber portion, l, as shown in Figure 2 is given by

$$l = \frac{L}{2}\left[1 - \frac{2}{\pi}\cos^{-1}\left(1 - \frac{\varepsilon}{\varepsilon_{max}}\right)\right] \tag{7}$$

where ε is the thickness strain and ε_{max} is the maximum thickness strain. The maximum thickness strain occurs when the fiber volume fraction is maximum. As pressure is applied to the preform as shown in Figure 3, the undeformed fiber portion decreases in length. The load applied to the peak of the fiber wave is supported by the undeformed portion of fiber. The fiber is assumed to behave like a beam clamped at both ends. Therefore, the force, F, required to deform the beam, Δ, at one end is given by

$$F = \frac{12EI\Delta}{l^3} \tag{8}$$

where E is the modulus of the fiber and I is the moment of inertia. The stress applied to the fiber is equal to the force, F, over the entire length of the fiber

$$\sigma = \frac{F}{d\,L/2} \tag{9}$$

and the strain, ε, is given by

$$\varepsilon = \frac{\Delta}{a+d_f} \tag{10}$$

Substituting equations (9) and (10) into (8) for a differential element results in the stress-strain relation for the compaction of the preform.

$$d\sigma = \frac{12EI}{l^3 d\,L/2}\left(a+d_f\right)d\varepsilon \tag{11}$$

Substituting equation (7) for l into the above equation yields the final compressibility of the fiber preform.

$$\frac{d\sigma}{d\varepsilon} = 3\pi E \frac{1 + a/d_f}{\left(d/d_f\right)\left(L/d_f\right)\left[1 - \frac{2}{\pi}\cos^{-1}\left(1 - \frac{\varepsilon}{\varepsilon_{max}}\right)\right]} \tag{12}$$

The resulting stress-strain curve was plotted by incrementing the fiber volume fraction and calculating the resulting stress (Figure 4). The result shows the nonlinear compressibility of the fiber preform. Appropriate input values can be chosen by correlation with experimental data. The input values used for the calculation were the following:

Fiber Modulus, $E = 234\ GPa$
Fiber Diameter, $d_f = 7\ mm$
Crimp Wavelength, $L = 0.52\ mm$
Initial Fiber Volume Fraction, $V_{fo} = 0.5$
Maximum Fiber Volume Fraction, $V_{fmax} = 0.72$

A. 2. Compaction of a General Fiber Preform

Now consider a fiber preform that is impregnated with liquid resin. The fiber compaction that occurs during processing of composites includes elastic deformation of the fiber network in conjunction with resin flow as the matrix material is displaced. Assuming the resin behaves like a Newtonian fluid with known viscosity, μ, field equations have been developed for the compaction of a general fiber preform.

The control volume representing a general fiber preform is shown in Figure 5. As the preform is compacted, the resin is squeezed through the fiber network. The resultant drag on the fiber network is shown as arrows within the preform (Figure 5). The total stresses in the preform are made up of the fiber stresses and the resin pressure. The stress, σ_{ij}, at any point is then determined by the rule of mixtures

$$\sigma_{ij} = V_f \sigma_{ij}^f + V_m \sigma_{ij}^m$$
$$\sigma_{ij}^m = -p_m \delta_{ij} \tag{13}$$

where V_f and V_m are the volume fractions of the fiber and matrix, σ_{ij}^f and σ_{ij}^m are the fiber and matrix stresses, p_m is the resin pressure and δ_{ij} is the Kroenicker delta. The Kroenicker delta is used because the resin pressure acts only in the normal directions. Representing position within the preform by x_i and the drag due to resin flow as a body force, f_i, the equilibrium equation for the fiber network is

$$\frac{\partial\left(V_f \sigma_{ij}^f\right)}{\partial x_j} + f_i = 0 \tag{14}$$

and the equilibrium equation for the matrix is written

$$\frac{\partial\left(V_m p^m\right)}{\partial x_j} + f_i = 0. \tag{15}$$

The stiffness of the fiber network is determined from the fiber compaction analysis and denoted C_{ijkl}^f. However, the compressibility of the fiber network is valid transverse to the fibers only. The axial stiffness is determined by the fiber stiffness itself. Also, the transverse compressibility is a function of the fiber volume fraction. The constitutive relation for the fiber network is given by

$$V_f \sigma_{ij}^f = C_{ijkl}^f\left(V_f\right)\varepsilon_{kl}^f \tag{16}.$$

The drag due to resin flow through the fiber network is determined by Darcy's law

$$f_i = \frac{1 - V_f}{K_i}\mu\left(v_i^m - v_i^f\right) \tag{17}$$

where Ki is permeability and v^m and v^f are the respective velocities of the matrix and the fiber.

The relationship between the displacements of the fibers and matrix is determined by the mass balance. The mass conservation relationship for the resin flow through the volume of the fiber network is

$$\frac{d}{dt}\int_{V_{\text{fiber net}}} \rho_m V_m dV = -\int_{\delta V_{\text{fiber net}}} \rho_m\left(v_i^m - v_i^f\right)n_i dS \tag{18}$$

where ρ_m is the density of the resin. Also, the fiber mass within the volume remains constant as given by

$$\frac{d}{dt}\int_{V_{\text{fiber net}}} \rho_f V_f dV = 0. \tag{19}$$

Therefore, the flow of the matrix is independent of position.

$$\frac{\partial v_i^m}{\partial x_i} = 0 \tag{20}$$

These general equations can be applied to many composite fabrication processes by making appropriate assumptions and applying boundary conditions. Two cases will be briefly discussed.

A. 3. One-dimensional Compaction

During autoclave curing of a flat laminate, as pressure is applied resin flow occurs primarily through the thickness. Figure 6 shows pressure being applied to a flat laminate in the z-direction. Modeling this is accomplished by simplifying the equations for compaction of a general fiber preform to one-dimension. Therefore, eliminating the indices, the equlibrium equations are written

$$\frac{\partial (V_f \sigma^f)}{\partial z} + f = 0 \tag{21}$$

$$\frac{\partial ((1-V_f)p^m)}{\partial z} + f = 0 \tag{22}$$

Also, the constitutive equations are simplified by applying compaction in only one direction. Therefore, the modulus, E_f, is determined from the compressibility of the fiber preform. The constitutive relations are given by

$$V_f \sigma^f = E_f(V_f)\frac{\partial u^f}{\partial z} \tag{23}$$

$$f = \frac{1-V_f}{K_T}\mu(v^m - v^f) \tag{24}$$

where K_T is the permeability transverse to the fibers. Finally, the continuity condition yields the following equations

$$\frac{\partial V_f}{\partial t} = -V_f \frac{\partial v^f}{\partial z} \tag{25}$$

$$\frac{\partial v^m}{\partial z} = 0. \tag{26}$$

Combining all of the above equations results in three partial differential equations.

$$\frac{1-V_f}{K_T}\mu\frac{\partial u^f}{\partial t} = E_f\frac{\partial^2 u^f}{\partial z^2} \qquad (27)$$

$$\frac{\partial p_m}{\partial z} = \frac{\mu}{K_T}\frac{\partial u^f}{\partial t} \qquad (28)$$

$$\frac{\partial V_f}{\partial t} = -V_f\frac{\partial v^f}{\partial z} \qquad (29)$$

These equations can be solved simultaneously to simulate the time dependent response of a fiber preform to an external pressure. Further equations can be added to include the effects of cure kinetics and heat transfer. The boundary conditions required to solve the above equations are given by

$$u^f = v^f = v^m = 0 \quad \text{at } z = 0 \qquad (30)$$

and

$$p_m = 0, \ V_f\sigma^f = -p_a \quad \text{at } z = h. \qquad (31)$$

A. 4. Compaction of Filament-Wound Cylinders

The equations for the compaction of a general fiber preform can also be applied to filament winding of cylindrical structures. During winding, continuous bands of resin impregnated fibers are wrapped onto a rotating mandrel. For accurate placement of fiber tows on the mandrel and to improve compaction, a tensile force called the winding tension is applied to the fiber tows. The winding tension exerts radial pressure on the previously wound layers and compacts the cylinder. Figure 7 shows a filament-wound cylinder with internal and external pressure being applied. External pressure is applied whenever a new layer is wound or when put into an autoclave. Internal pressure is due to the support that the mandrel provides for the cylinder before it is cured. Cylindrical coordinates are shown in the figure.

The main change required to apply the general compaction equations to filament winding is the transformation to cylindrical coordinates. The equilibrium equations for cylindrical coordinates are given as

$$\frac{\partial}{\partial r}\left(V_f\sigma_r^f\right) + \frac{V_f\left(\sigma_r^f - \sigma_\theta^f\right)}{r} + f_r = 0 \qquad (32)$$

$$\frac{\partial}{\partial r}\left(V_m p_m\right) + f_r = 0 \qquad (33)$$

where f_r represents the drag force in the radial direction. The drag force is derived from Darcy's law

7

$$f_r = \frac{V_m}{K_T} \mu \left(v_r^m - v_r^f \right) \tag{34}$$

where v_r is the velocity in the radial direction. The stress-strain relations in cylindrical coordinates are

$$V_f \sigma_r^f = Q_{rr} \frac{du_r^f}{dr} + Q_{r\theta} \frac{u_r^f}{r} \tag{35}$$

$$V_f \sigma_\theta^f = Q_{r\theta} \frac{du_r^f}{dr} + Q_{\theta\theta} \frac{u_r^f}{r} \tag{36}$$

where Q represents the stiffness in the subscripted directions. The stiffness in the radial direction can be found from the nonlinear compressibility analysis and the axial stiffness can be determined from the fiber properties. A process simulation can be developed from the above equations for each of the stages of filament-winding. During winding, application of each new layer requires changing the boundary conditions and during curing, heat transfer and cure kinetics equations should be solved simultaneously.

B. Filament Winding Experiments

Experimental work has been used to both verify and complement the analytical work. Because existing models have been accompanied by very little experimental correlation, key assumptions have not been justified. Previously, the stress development during winding of dry glass fiber was investigated. A linear elastic analysis was used to find an effective radial modulus by fitting the prediction to the experimentally measured pressure at the mandrel surface. The ratio of the hoop modulus to the inferred radial modulus was in the order of 10^4, indicating a very high anisotropy. The very low radial modulus resulted in an asymptotic increase of mandrel pressure after only about 6 layers were wound.

Although the linear elastic analysis described dry winding very well, extending the analysis to winding with prepreg material is dependent on the amount of stress relaxation that occurs due to resin flow. Because very high viscosity resins are used in prepreg materials this relaxation is usually assumed to be negligible. But, the fiber migration and stress relaxation due to resin flow is considered the most important issue regarding fiber buckling. Therefore, the effect of stress relaxation during the filament winding process was investigated. The main objectives were to determine the extent of stress relaxation during processing and to relate processing conditions to final quality in thick tubes.

B. 1. Experimental Procedure

Filament winding was carried out on an Entec filament winder using Hercules 12K, AS4-3501-6 carbon prepreg tows. The prepregs had a fiber volume fraction of 61.0%. The tow was nominally 5.08 mm wide and 0.25 mm thick.

8

The prepreg tow was wound on an aluminum mandrel over its 50.8 *mm* mid-section which was bounded by a pair of end plates. The mandrel was 57.7 *mm* in outside diameter, 3.4 *mm* thick, and 203 *mm* long. The end plates were fitted onto the mandrel to prevent the wound tow from slipping. These end plates were machined out of transparent plexiglass sheets to enable on-line monitoring of fiber buckling at an edge.

Winding tension was applied using an American Sahm tensioner. The winding tensions used ranged from 13 *N* to 34 *N*. However, during each winding series the winding tension was kept constant throughout. A full layer of winding required 9.85 revolutions and a constant rotational speed of the mandrel was used for each cylinder. Cylinders were wound at three speeds, 3.5 *RPM*, 10.5 *RPM* and 31.5 *RPM*. The test was only stopped if the tow being laid became crimped or flipped over. Cylinders of up to 60 layers were wound.

Curite process pressure sensors were used to measure the mandrel pressure. The mandrel/sensor arrangement is shown in Figure 8. One gage and its accompanying thermocouple was attached on the mandrel surface and an additional thermocouple was used to measure the ambient temperature. The gages were 15 *mm* wide, 23 *mm* long, 0.3 *mm* thick, and had a 10 *mm* diameter active area. They were designed for pressures up to 1.4 *MPa*. The thermocouple and pressure sensor wires were connected to an Omega 900 data acquisition system through a slip ring. The experimental setup is shown in Figure 9.

After winding, the wound cylinder sat for two hours to measure any pressure change while sitting. The cylinder was then placed in an oven at 100 *C* for two hours and then allowed to cool to room temperature. Pressure data was taken throughout the heating and cooling of the cylinder.

Finally the part was fully cured using Hercules' suggested cure cycle. No external pressure was applied. The part was cured as follows: A ramp of 1.7 to 2.8 *C·min* to 115.6 *C*, a 60 to 70 minute dwell at 115.6 *C*, a 1.7 to 2.8 *C·min* ramp to 176.7 *C*, maintained at 176.7 *C* for 120 minutes and temperature decreased 2.8 *C·min* to 93.3 *C* and layup removed.

B. 2. Results

The pressure at the interface of the mandrel and composite is a basic characteristic of the filament-wound structure. The winding tension applied to the prepregs builds up the pressure on the mandrel and helps consolidate the cylinder. To allow mandrel removal by the end of the technological process, the pressure must eventually be relaxed. Subsequently, pressure sensors were used to monitor mandrel pressure throughout each stage of the filament winding process.

Winding with prepreg tows showed some significant differences from the results obtained with the dry fiber. Figure 10 displays the mandrel pressure during winding of a 30 layer cylinder at 3.5 *RPM* with winding tension of 22.25 *N*. Due to the small size of the pressure sensors in comparison to the winding length, a stepwise increase in pressure is seen as additional layers were wound. Because, the sensors are located midway between the endplates, the payout eye traverses to the end of the mandrel and back before an additional layer is wound. It takes 9.85 revolutions to wind a complete layer, therefore there is about 2.8 minutes between winding of layers. Because the machine was stopped

occasionally in the event of misplaced tows, this time was even greater for some layers. The pressure decrease due to the stress relaxation was very rapid at first and slowly tapered off.

The maximum mandrel pressure was reached after 6 layers were wound. After this point, the pressure decrease due to stress relaxation exceeded the pressure increase due to the winding of additional layers. Subsequently, a net decrease in mandrel pressure occurred although layers were continuously being added. Even though there was little pressure change over the winding of the last several layers, small pressure jumps were evident as each layer was wound. The final mandrel pressure after winding of 30 layers was less than 0.15 *MPa* and approximately the same as the pressure after only 1 layer was wound.

Because stress relaxation was seen to occur during winding with prepreg tow, the rate of winding is an important processing parameter. Winding at slow speeds, nearly complete stress relaxation occurs during winding. Alternatively, at fast winding speeds, little stress relaxation would be expected during winding and would have to occur once the part has been fully wound. The difference between these two approaches to winding were investigated to determine how winding speed affects the final quality in wound cylinders. In addition, winding tension was varied to study its significance as well.

Figures 11 and 12 show the variation in mandrel pressure with time for cylinders wound at 10.5 *RPM* and 31.5 *RPM*, respectively. At each winding rate, cylinders were wound with winding tensions of 13.35, 22.25 and 33.15 *N*. Significant differences are evident due to varying winding speed as well as winding tension. Of course, mandrel pressures were greater with increasing winding tensions due to greater compaction. Also, as expected, much greater relaxation occurred in the slow winding than in the fast winding. The significant difference in relaxation is due to the fact that when winding at 10.5 *RPM* there was 56 seconds between layers as compared to only 19 seconds at 31.5 *RPM*. Nevertheless, the greatest rate of relaxation occurs just after the layer is placed and then it slowly tapers off. At both 10.5 *RPM* and 31.5 *RPM* relaxation in the wound layer was still occurring when the next layer was wound. Still, the relaxation rate was tapering off as additional layers were added at 10.5 *RPM*. Therefore, similar results were found due to winding at 10.5 *RPM* and 3.5 *RPM*.

After winding, mandrel pressure was continuously monitored for as long as relaxation was evident. Figures 13 and 14 show the mandrel pressure throughout the entire time of winding and storage for winding speeds of 10.5 and 31.5 *RPM*. At 10.5 *RPM*, very little change in mandrel pressure occurred after winding. However, because less relaxation occurred during actual winding at 31.5 *RPM*, relaxation continued after winding. Nevertheless, final mandrel pressures were still higher after storage for 31.5 *RPM* than for 10.5 *RPM*. Therefore, greater relaxation was required during curing.

After complete relaxation occurred at room temperature, the cylinders were placed in an oven for curing. However, before following the recommended cure cycle, the effect of an elevated temperature on stress relaxation was investigated. Although elevating temperature causes a drop in viscosity and increases flow, higher temperatures cause an increased rate of curing. In an effort to isolate relaxation effects, a temperature was chosen that was high enough to accelerate relaxation, but low enough to maintain a fairly

constant viscosity. Therefore, based on viscosity data presented in [11], 100 C was chosen as the dwell temperature.

Figures 15 through 18 show the change in mandrel pressure during heating for three of the tubes. The high coefficient of thermal expansion of aluminum caused an increase in pressure as the mandrel expanded. Thus, mandrel pressure behaved very similar to part temperature throughout the test. However, note that during the initial ramp a difference occurred. While initially mandrel pressure increased with temperature, it dropped off after 10 minutes or so in all cases. The relaxation lasted several minutes and then the pressure increase continued. Another relaxation occurred before the desired temperature was reached. After the part was cooled to room temperature, mandrel pressure was less than half of its original value. In all cases, relaxation was completed during the initial ramp.

The cylinders were later cured by following Hercules' suggested cure cycle with no augmented pressure. While it is difficult to compare the data obtained during heating of each of the cylinders, it will be useful for correlation with analytical results.

Figure 19 shows the effective layer thicknesses (i.e. the total thickness divided by the number of layers) for each of the winding conditions. Tighter winding was achieved with higher winding tensions resulting in smaller effective layer thicknesses. However, more drastic was the increase in consolidation with the slower winding speed used. Note that the layer thickness due to the highest tension at the fastest speed (33.15 N, 31.5 RPM) was essentially the same as the layer thickness due to the lowest tension (13.35 N) at 10.5 RPM.

The quality of the wound tubes were examined by cutting the parts in half and observing the cross-sections. Large inter-tow gaps were evident in poorly consolidated cylinders but no wavy fiber layers occurred. Fiber orientations were observed in more detail by polishing the cross-sections and examining using an optical microscope. Figure 20 is a photomicrograph taken of the cross-section of the cylinder wound at 10.5 RPM with 33.15 N winding tension. Although this cylinder had relatively good consolidation, large gaps could be seen in the cross-section.

Although wavy fiber layers were not evident in the wound cylinders, fiber waviness occurred in the axial direction. In the photomicrograph fiber orientation can be ascertained by comparing the visible regions of the fibers. Viewing the sides of the fibers they appear as long thin lines and when the fibers are directed out of the plane the elliptical cross-sections are visible. When both the sides and the ends of fibers can be seen within the same layer, axial fiber waves are apparent.

Fiber waviness was compared for all of the winding conditions studied by counting the number of fiber waves over a 1 cm length. Shorter fiber wavelengths were visible in tubes wound with greater winding tensions while winding speed had no apparent effect.

B. 3. Experimental Correlation

Numerical simulations were performed to calculate the stress development during winding using the relaxation analysis detailed in [1]. A computer program was written to combine a linear elastic winding model with the stress relaxation model to predict the drop in mandrel pressure between winding layers. Figure 21 shows the variation of the

normalized mandrel pressure during winding calculated from the numerical simulation and measured during the winding of a tube at 10.5 *RPM* with 22.25 *N* winding tension. The parameters that were varied to fit the experimental results were the radial modulus and the creep strain rate. The radial modulus affects the number of layers it takes for the mandrel pressure to reach maximum and the creep strain rate affects the amount of relaxation that occurs. Note that while the simulation results follow the general trend of the experimental data, the final mandrel pressure is incorrect. Resin flow during processing is a function of the fiber volume fraction of the preform. As the fiber volume fraction increases, the resin flow decreases causing the stress relaxation to stop. However, for the stress relaxation analysis, stress relaxation is a function only of the radial stress within the cylinder. Therefore, stress relaxation continues until the mandrel pressure is zero. The following input values were used for the simulation

$$\text{Transverse Modulus, } E_T = 1.03 \times 10^6 \, MPa$$
$$\text{Radial Modulus, } E_R = 34.45 \, MPa$$
$$\text{Creep Constant, } K = 7.26 \times 10^{-4} \, (MPa \cdot sec)^{-1}$$

III. FUTURE ACTIVITIES

A. Analytical Model Development

An analytical model has been developed for fiber compaction and resin flow. This model can be used to simulate autoclave curing or filament winding with inclusion of heat transfer and cure kinetics. Well developed models already exist for predicting the temperature distribution and degree of cure for composites processing. These can be combined with the fiber compaction and resin flow model.

Combining all of the equations describing the processing results in several partial differential equations. To solve these equations, a numerical algorithm needs to be developed. Because simple geometries will be used, the finite difference method has been found to be successful. In this case, the system can be discretized and all of the derivatives can be written as finite differences. The key issues regarding the use of this method are the stability and precision of the solution. Appropriate input parameters will be determined from the filament winding experiments as well as published data on autoclave curing. Also, experimental correlation will be used to evaluate the models.

B. Filament Winding Experiments

The filament winding experiments detailed in this report are the beginning of a systematic study to determine how processing conditions affect fiber waviness. The information generated by this study will be used to guide the analytical work and the data will be used for experimental correlation. The stress relaxation during filament winding has been investigated throughout the entire process. Detailed measurements of the fiber waviness due to each winding condition will be acquired using digital image analysis from photomicrographs. Also, other processing conditions will continue to be investigated.

The major conditions to be studied are the effect of winding angle, winding tension, and *in-situ* heating during tow placement.

C. Compressive Strength of Thick Composites

The compressive strength of thick composites will be related to processing conditions for thick laminates as well as thick filament-wound cylinders. Laminates ranging from 5.0 to 25.0 *mm* are being fabricated using various cure cycles. These include suggested cure cycles from the material manufacturer as well as a real-time expert system controlled cure. These laminates will be monitored for quality and compression tested. The failure sequence will be monitored using a long distance microscope and video camera.

Filament-wound cylinders will also be compression tested. Each of the cylinders fabricated as part of the filament winding experiments will be tested. A fixture is being designed for these tests. Also, some cylinders will be sent to the Navy labs for hydrostatic testing. The failure sequence will be monitored using the long distance microscope for tests done in-house.

REFERENCES

1. Kempner, E.A. and Hahn, H.T., "The Effect of Radial Stress Relaxation on Fiber Stresses in Thick Filament-Wound Cylinders," To be published in the Proceedings of the 1993 International Conference on Composite Materials.

2. Altmann, H.C., "Formulas for Computing the Stresses in Center-Wound Rolls," *Journal of the Technical Association of the Pulp and Paper Industry (TAPPI)*, Vol. 51, 1968, p.176.

3. Monk, D.W., Lautner, W.K., and McMullen, J.F., "Internal Stresses Within Rolls of Cellophane," *TAPPI*, Vol. 58, 1975, p. 152.

4. Yagoda, H.P., "Resolution of a Core Problem in Wound Rolls," *ASME Journal of Applied Mechanics*, Vol. 47, 1980, p. 847.

5. Calius, E.P., Lee, S.Y., and Springer, G.S., "Filament Winding Cylinders: II. Validation of the Process Model," *Journal of Composite Materials*, Vol. 24, 1990, p. 1299.

6. Lee, S.Y. and Springer, G.S., "Filament Winding Cylinders: I. Process Model," *Journal of Composite Materials*, Vol. 24, 1990, p. 1270.

7. Spencer, B.E., "Prediction of Manufacturing Stresses in Thick-Walled Orthotropic Cylinders," PhD. thesis, 1988, The University of Nebraska-Lincoln.

8. Tarnopol'skii, Y.M. and Beil', A.I., "Problems of the Mechanics of Composite Winding," Chapter II in *Handbook of Composites, Vol. 4: Fabrication of Composites*, A. Kelly and S.T. Mileiko, Eds., Elsevier Science Publisher B.V., 1983, p.45.

9. Gutowski, T.G., Morigaki, T., and Cai, Z., "The Consolidation of Laminate Composites," *Journal of Composite Materials*, Vol. 21, 1987, p. 172.

10. Cai, Z., Gutowski, T.G., and Allen, S., "Winding and Consolidation Analysis for Cylindrical Composite Structures," *Journal of Composite Materials*, Vol. 26, 1992, p. 1374.

11. Lee, W.I., Loos, A.C., and Springer, G.S., "Heat of Reaction, Degree of Cure, and Viscosity of Hercules 3501-6 Resin", *Journal of Composite Materials*, Vol. 16, 1982, p. 510.
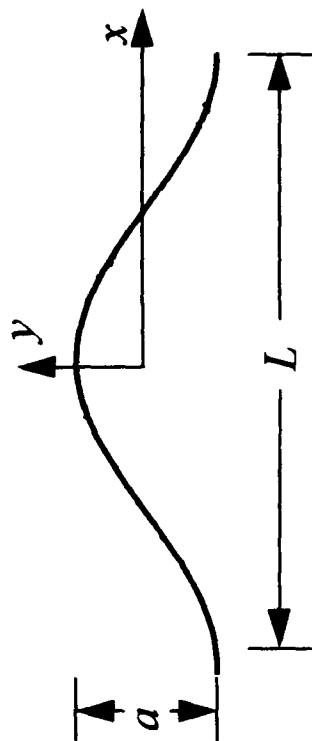
Figure 1. Initial fiber shape in fiber preform
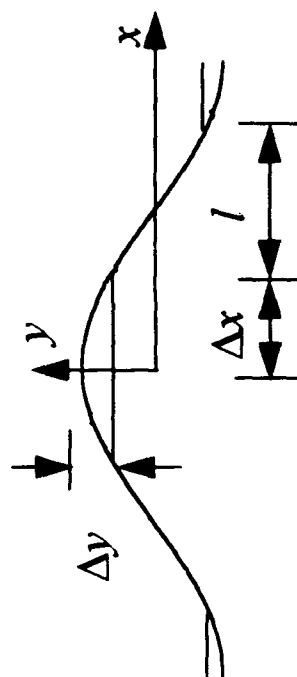
Figure 2. Fiber deformation during compaction

15
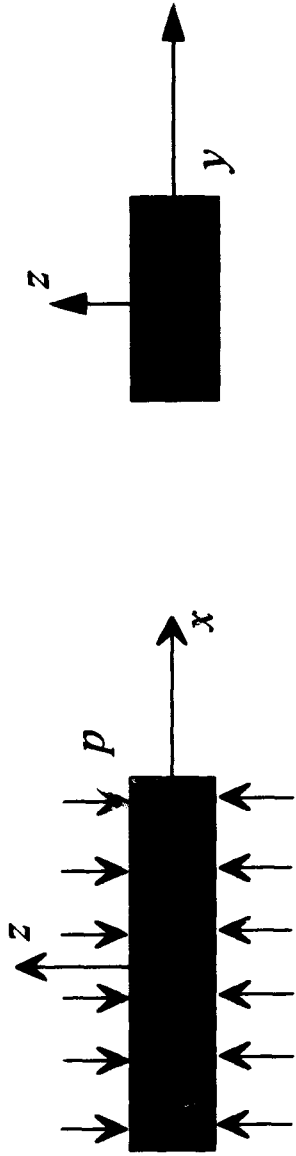
Figure 3. Compaction of a fiber preform
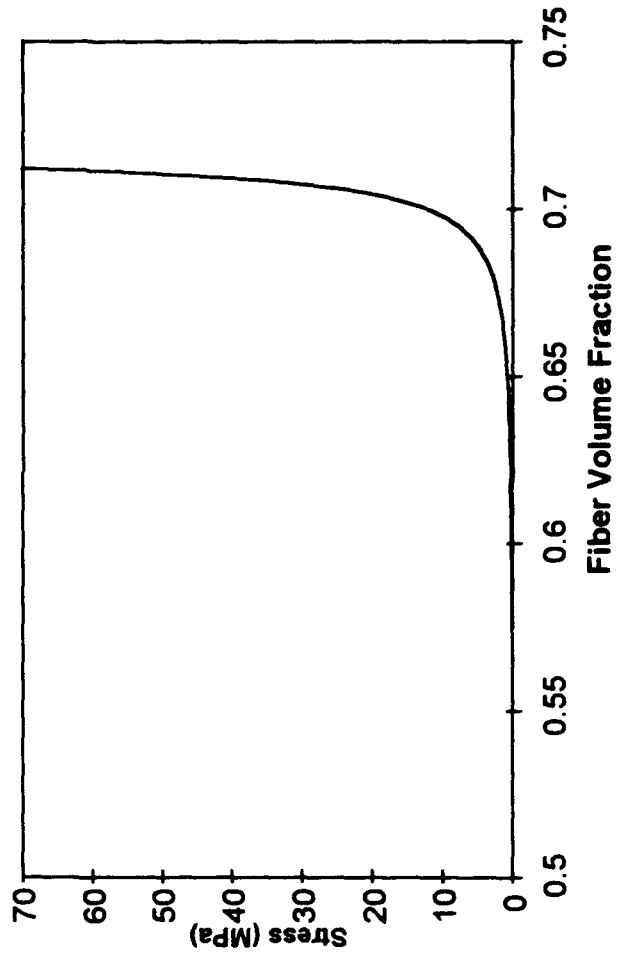
Figure 4. Nonlinear compressibility of fiber preform

16

$_f\sigma^f_{11} + d(V_f\sigma^f_{11})$

$_f\sigma^f_{11}$

Figure 5. Control volume of a general fiber preform

p_a

z

h

x
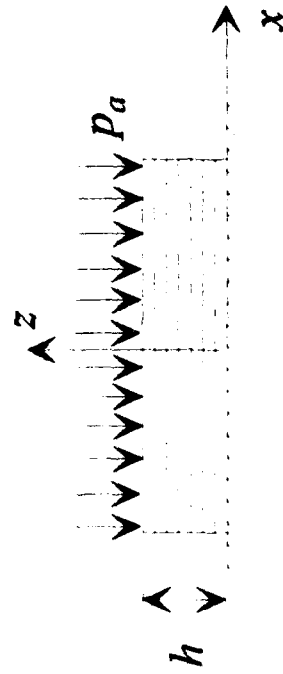
Figure 6. One-dimensional compaction

17
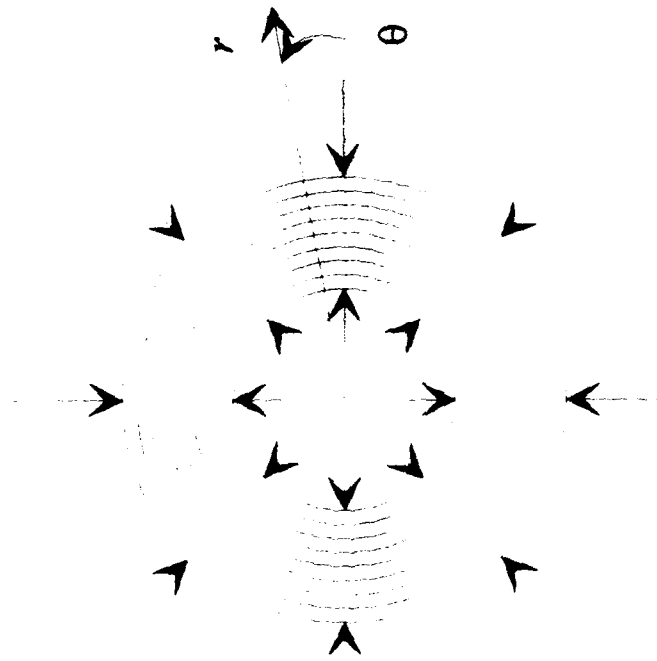
Figure 7. Compaction of a filament-wound cylinder

18

Clear Plastic Edge Dams

Sensors

Double-Sided
Tape

To Slip
Ring
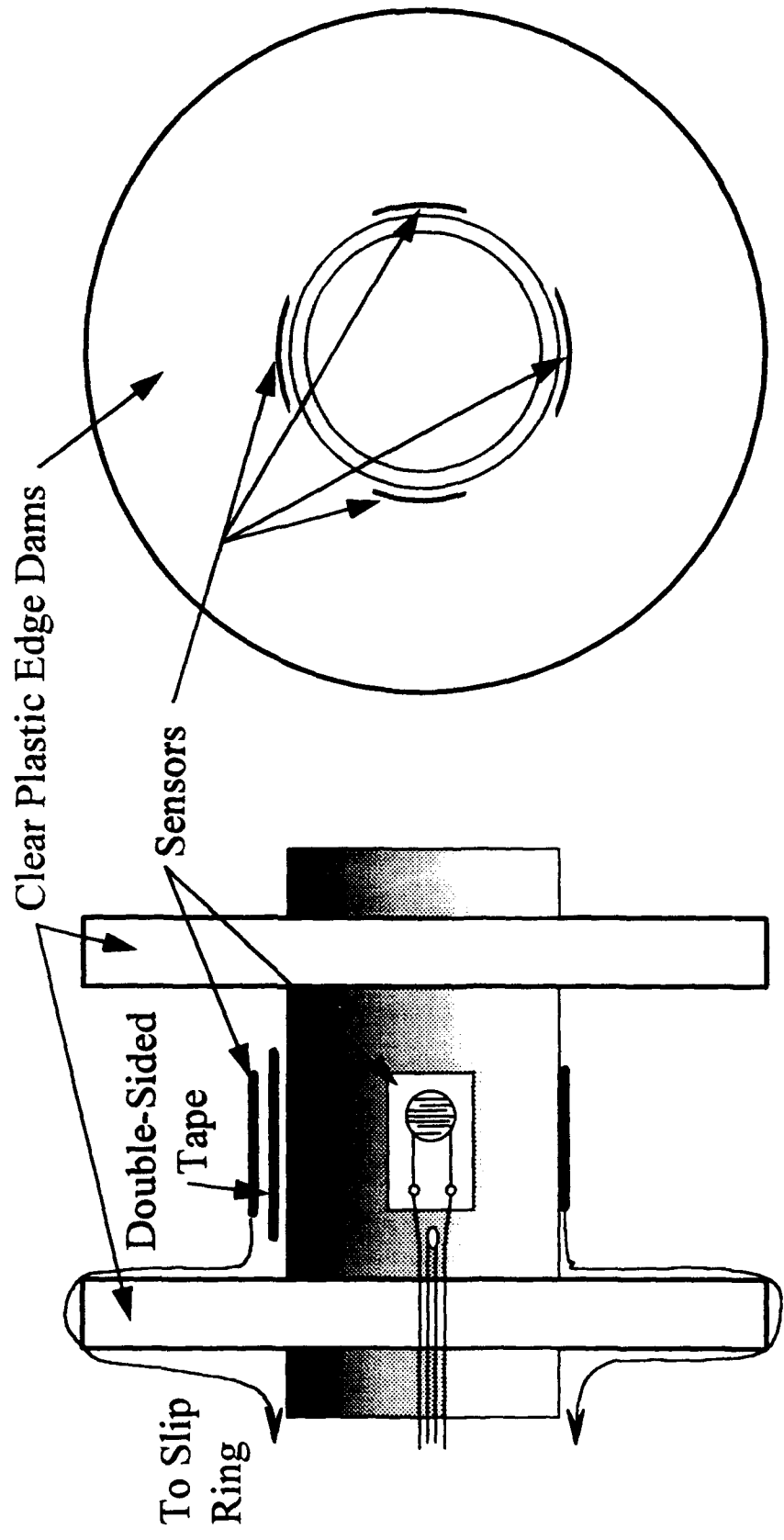
Figure 8. Mandrel/sensor arrangement

19
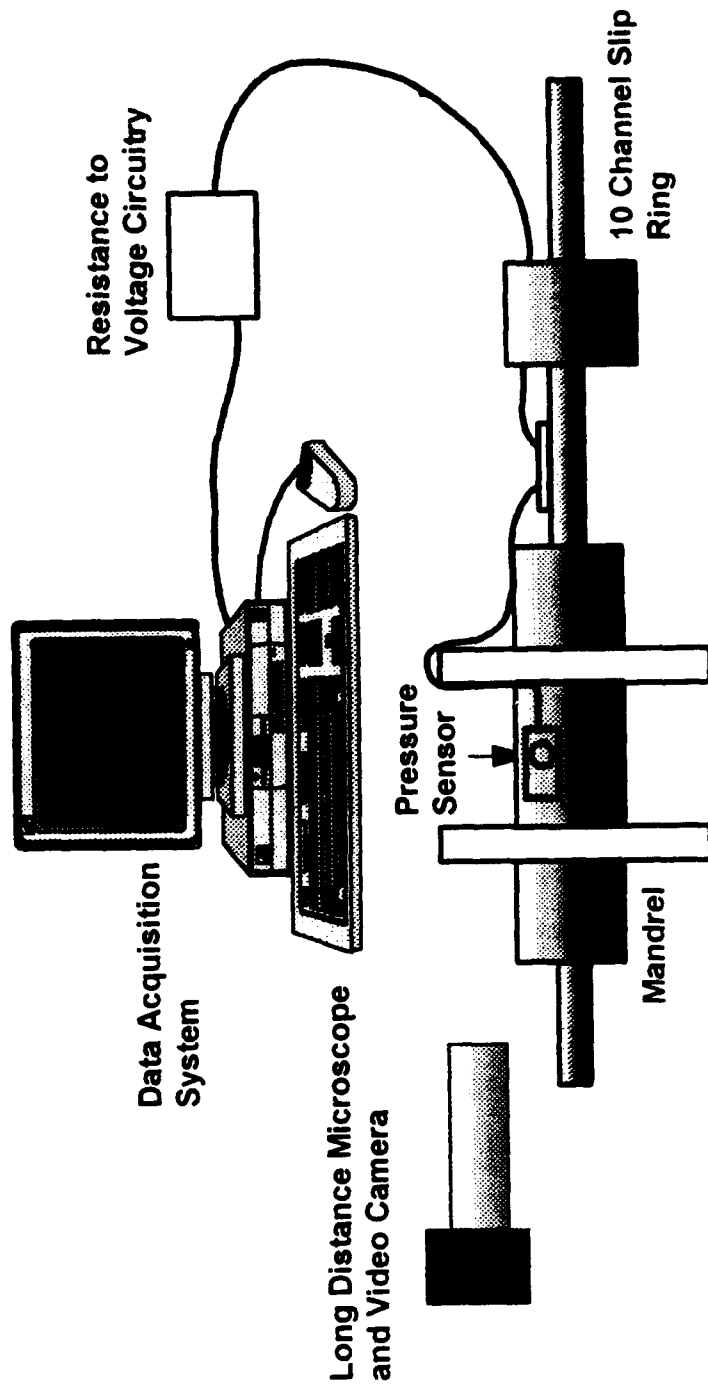
Figure 9. Experimental Setup

20
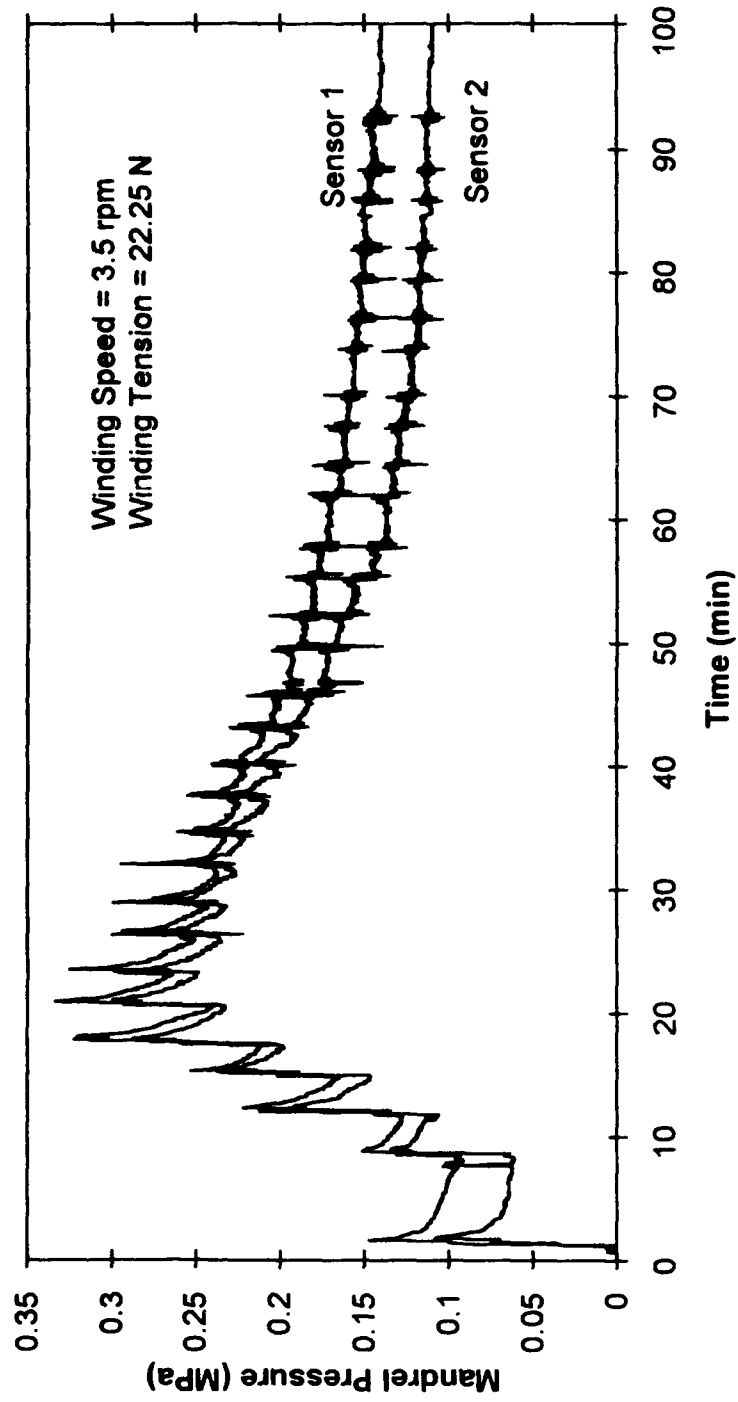
Figure 10. Change in mandrel pressure during winding

21
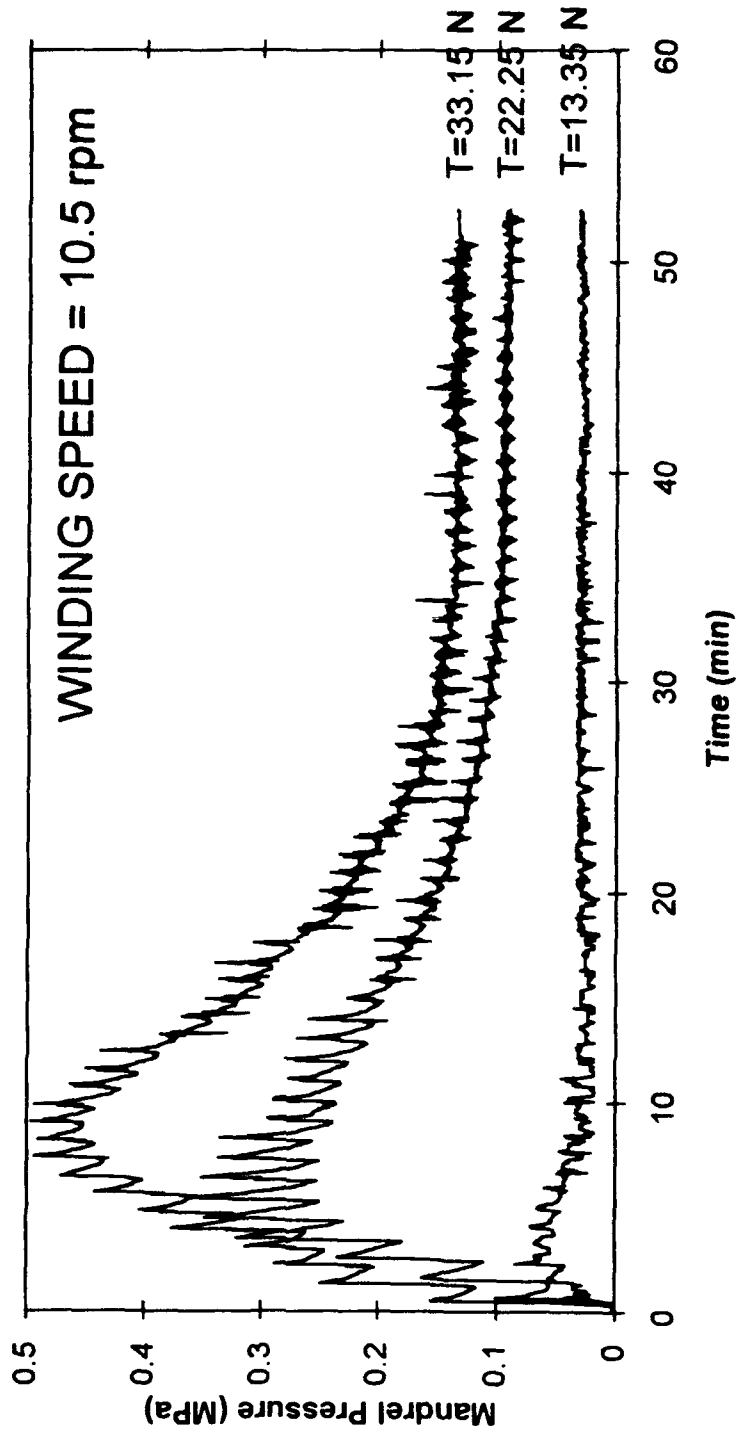
Figure 11. Change in mandrel pressure during winding. Winding speed = 10.5 *RPM*

22
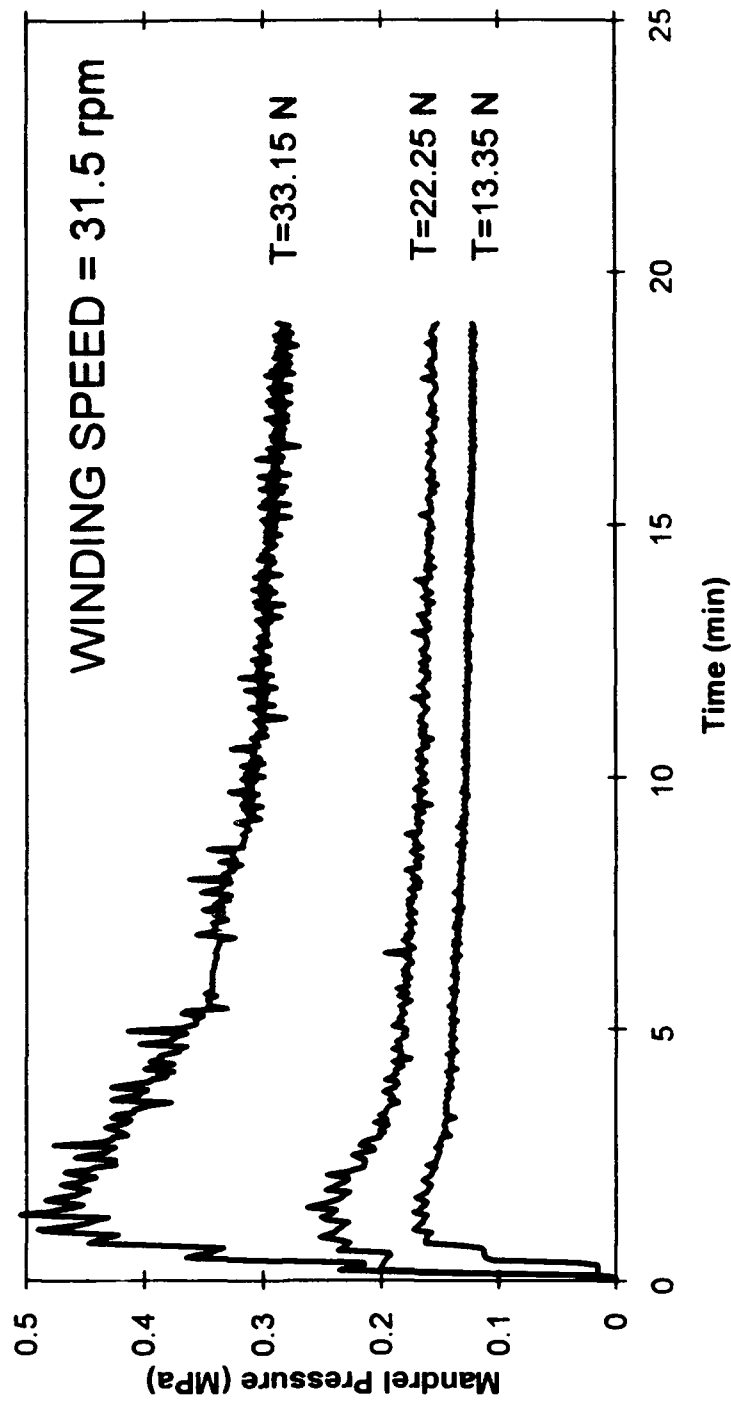
Figure 12. Change in mandrel pressure during winding   Winding speed = 31.5 *RPM*

23
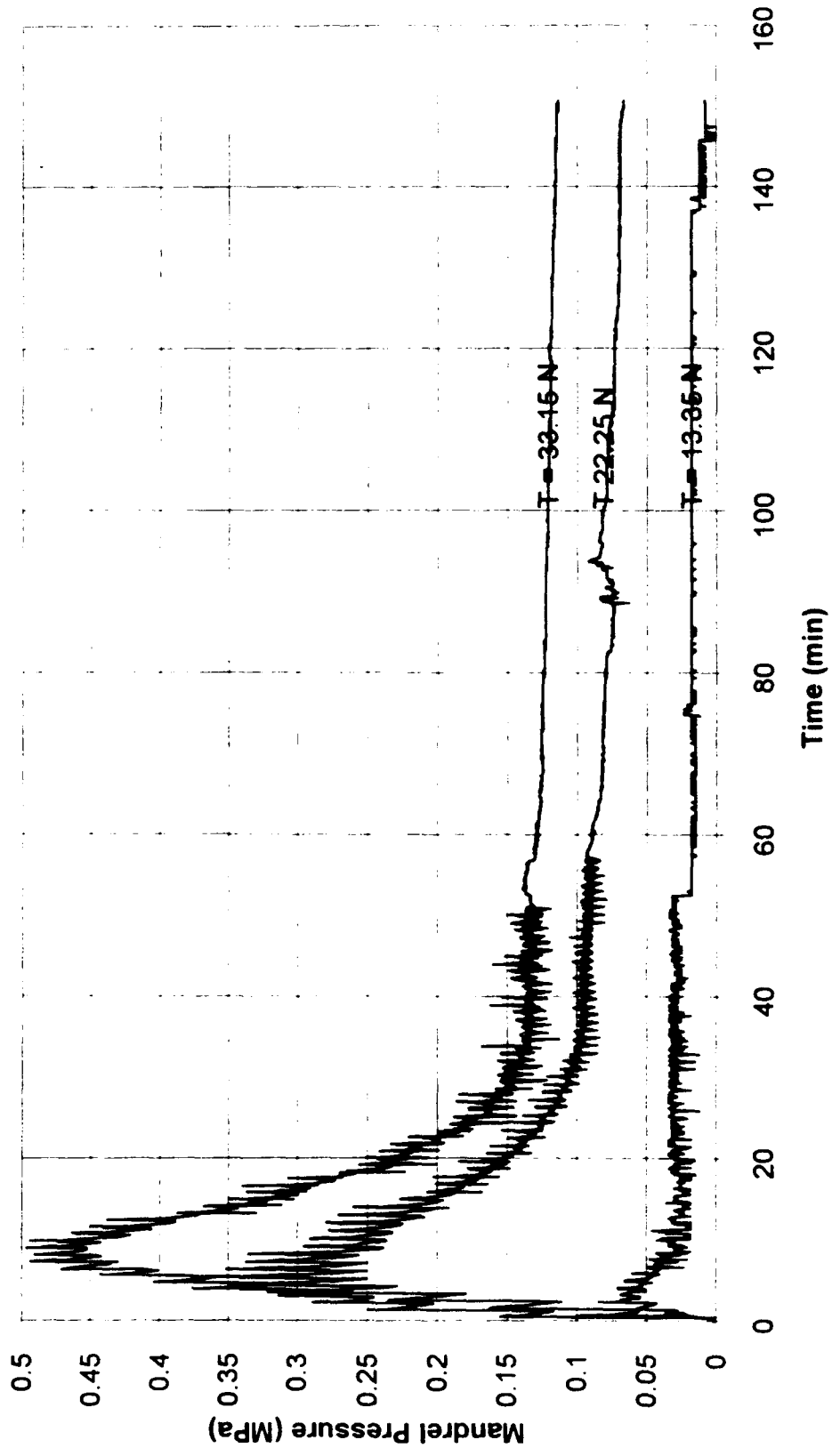
Figure 13. Change in mandrel pressure during winding and storage. Winding speed = 10.5 *RPM*

24
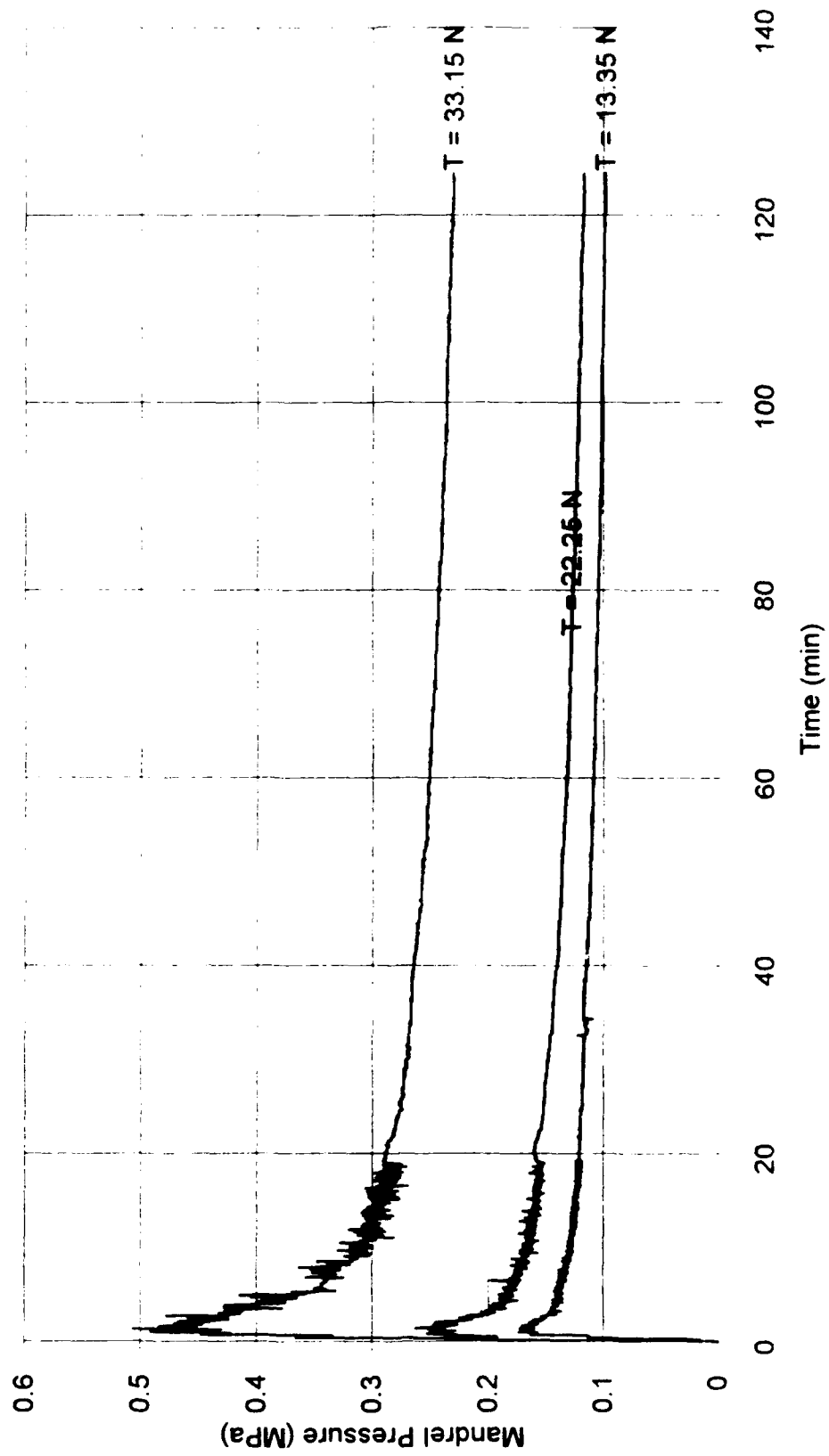
Figure 14. Change in mandrel pressure during winding and storage. Winding speed = 31.5 *RPM*
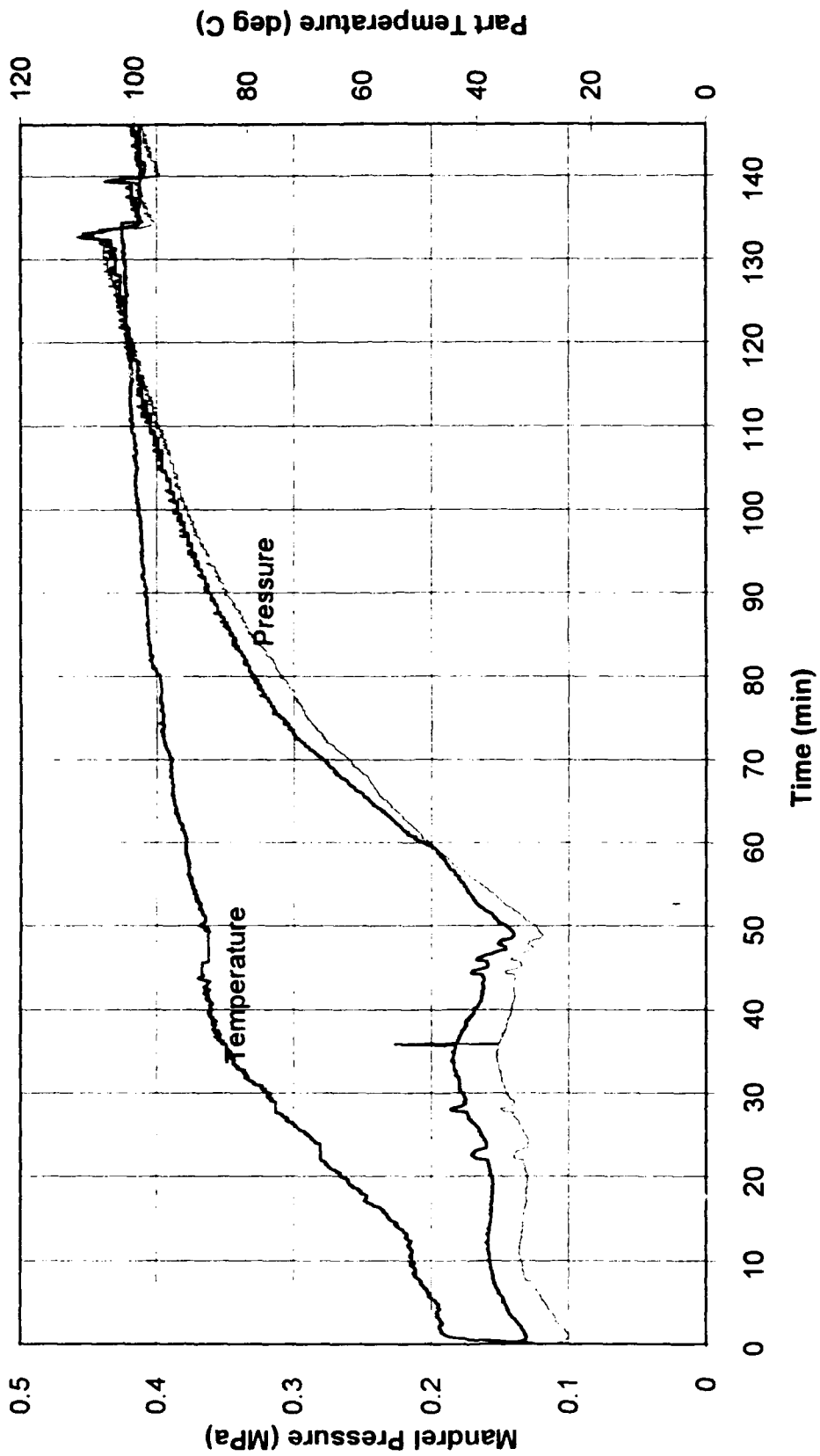
Figure 15. Change in mandrel pressure during 100 C dwell. T = 22.25 N, Winding speed = 3.5 RPM

26
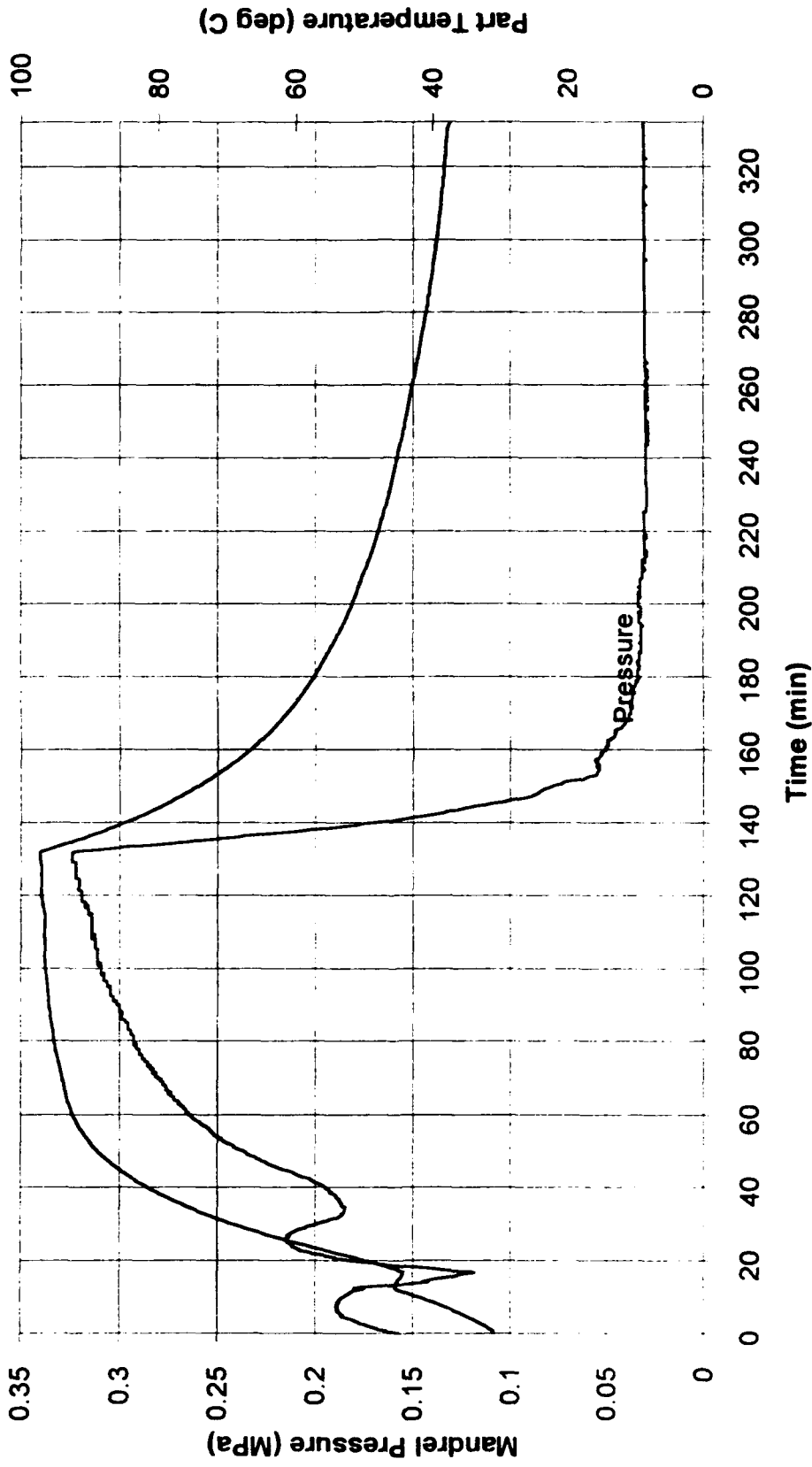
Figure 16. Change in mandrel pressure during 100 C dwell. T = 33.15 N. Winding speed = 10.5 *RPM*

27
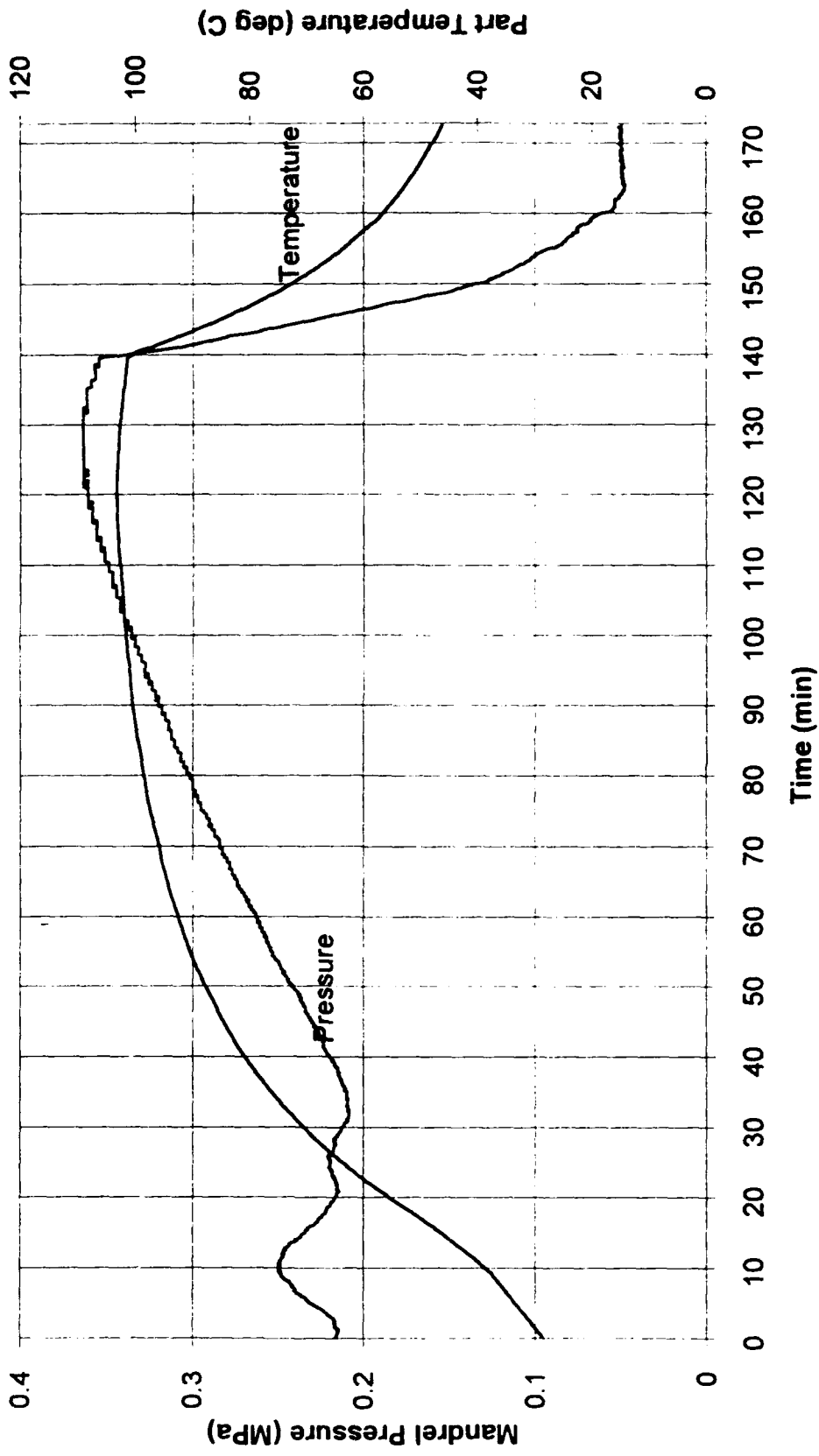
Figure 17. Change in mandrel pressure during 100 C dwell. $T = 33.15\ N$, Winding speed = 31.5 RPM

28
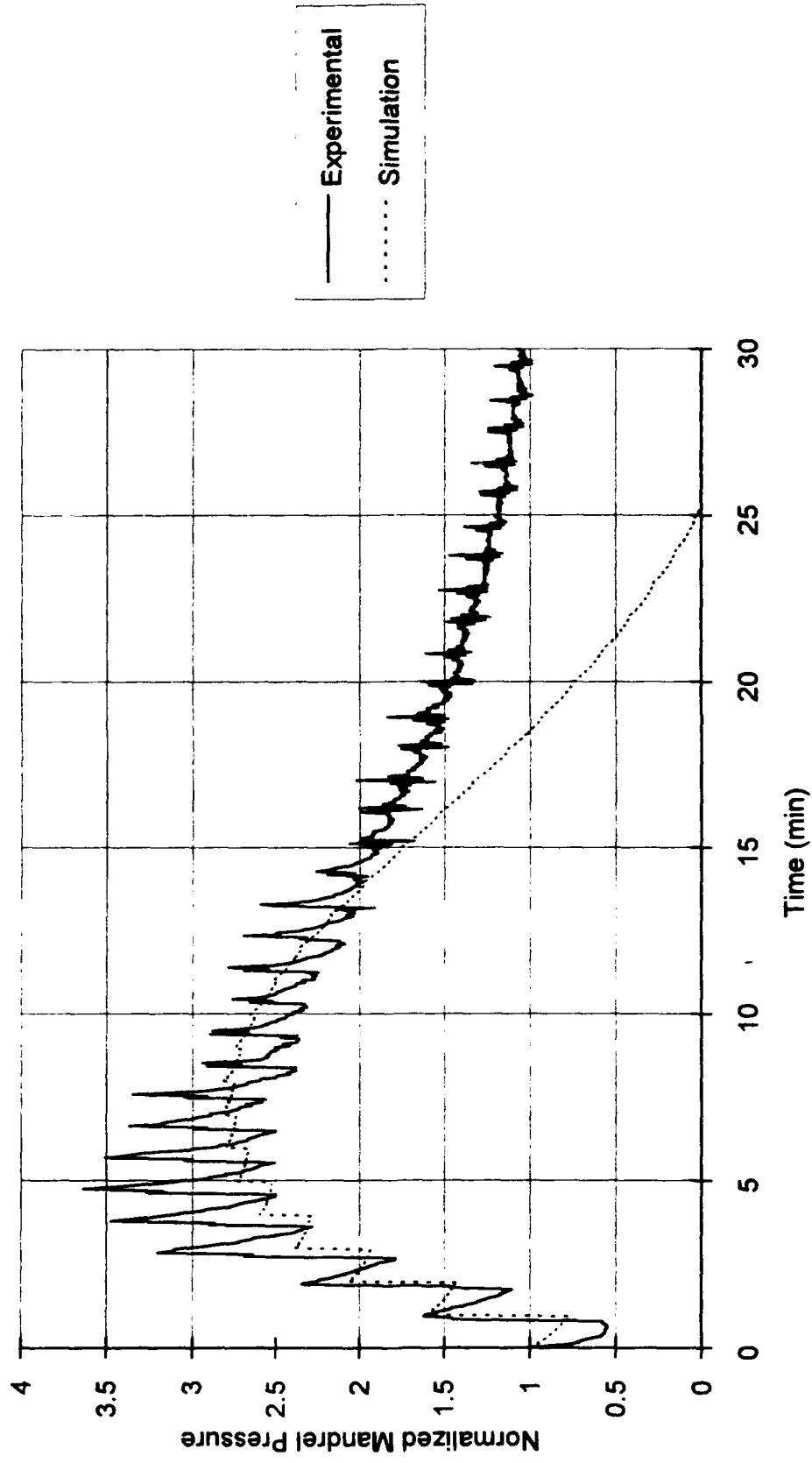
Figure 18. Experimental correlation with a winding simulation model including stress relaxation
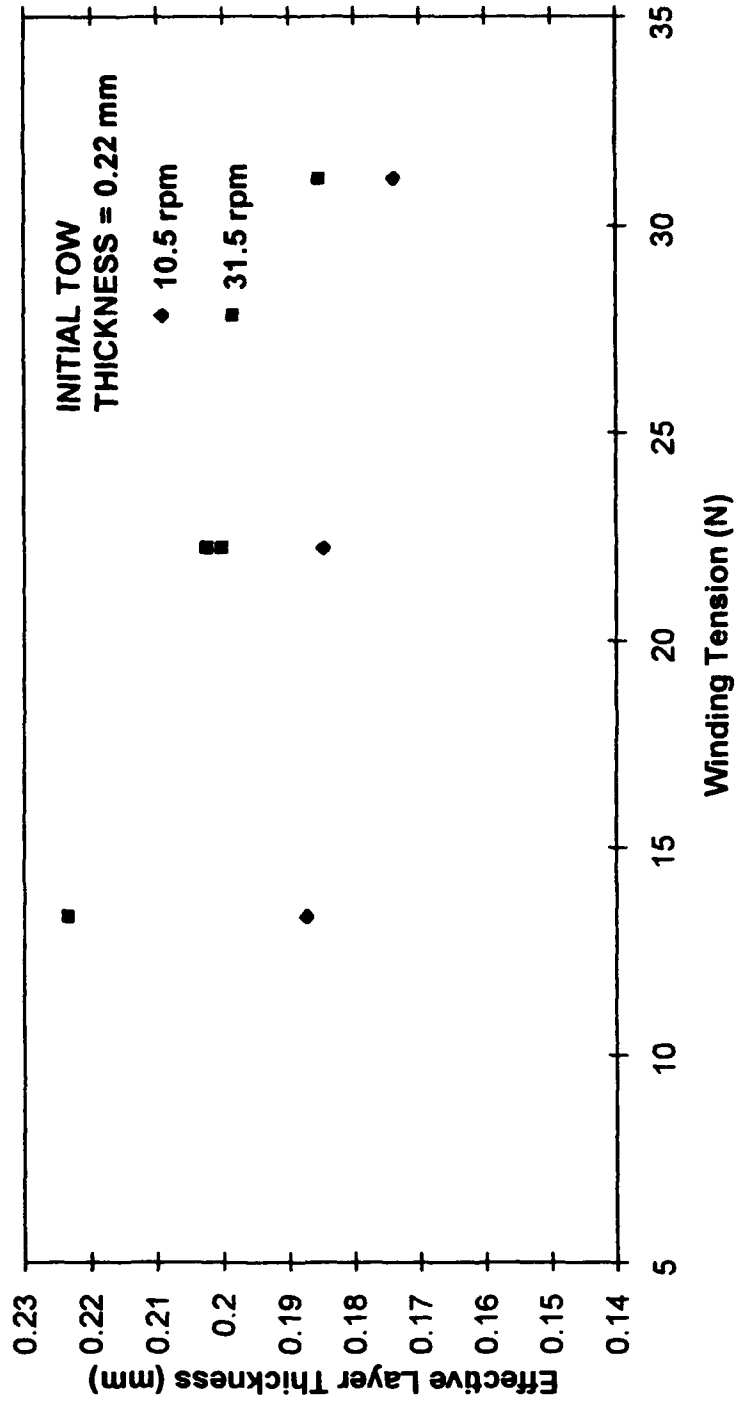
Figure 19. Effective layer thickness for each winding condition
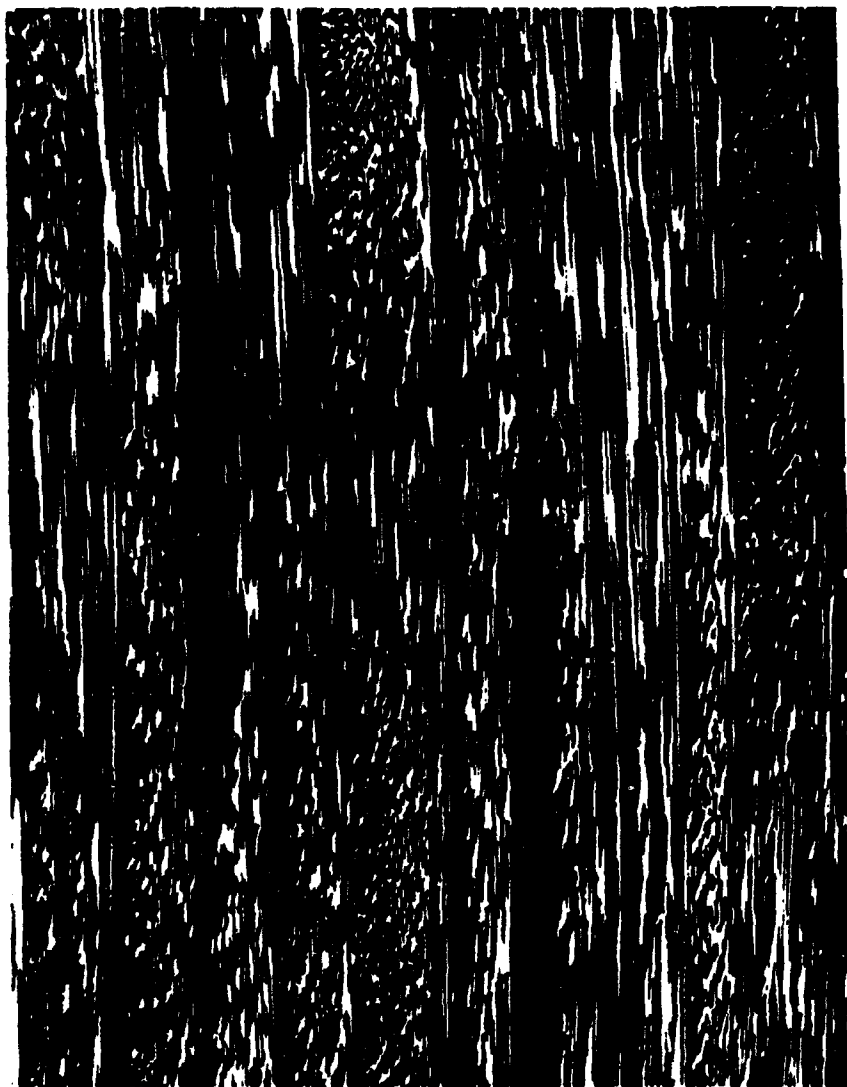
Figure 20. Photomicrograph of cylinder cross section, T = 33.15 *N*, Winding speed = 10.5 *RPM*

30

THE EFFECT OF RADIAL STRESS RELAXATION ON FIBER STRESSES IN THICK FILAMENT-WOUND CYLINDERS

Evan A. Kempner and H. Thomas Hahn
University of California, Los Angeles
Los Angeles, CA 90024-1597

ABSTRACT

The stress redistribution due to fiber motion in thick, filament-wound cylinders is analyzed in the present paper. An initial stress distribution in the wound cylinder is calculated based on an elastic analysis. The effect of subsequent fiber motion is described by a radial creep strain rate which is proportional to the radial stress. Numerical simulations have been performed for the stress redistribution in cylinders wound with winding tensions varying from 11.0 N to 44.5 N. The compressive axial fiber stress is shown to increase upon relaxation of compressive radial stress, the change increasing with the winding tension. Unfortunately, the new stress distributions favor fiber buckling.

Keywords: filament winding, fiber buckling, residual stresses, stress relaxation

1. INTRODUCTION

Filament winding is the predominant manufacturing process for composite cylinders. While winding of thin cylinders is fairly straightforward, fabrication of thick cylinders often results in wavy fiber tows which are detrimental to the compressive strength. Thus the stress development during the entire filament winding process must be known if optimum processing conditions are to be chosen for thick cylinders.

The main stages of the filament winding process during which fiber wrinkling may occur are the winding and curing. During winding, continuous bands of resin impregnated fibers are wrapped onto a rotating mandrel. In wet winding, fiber tows are pulled through a liquid resin bath for impregnation whereas fibers preimpregnated with B-staged resin are utilized in dry winding. For accurate placement of fiber tows on the mandrel and to improve compaction, a tensile force called

the winding tension is applied to the fiber tows. The winding tension exerts radial pressure on the previously wound layers and compacts the cylinder. Compaction occurs primarily because fibers are not completely straight. The radial fiber motion associated with the compaction reduces the tension in the fibers. When the cylinder is thick, the axial fiber stress inside the cylinder can even be compressive, causing the fibers to buckle. However, the very radial pressure that causes compaction also supports the fibers and helps prevent buckling. Thus, the compressive axial fiber stress and the compressive radial stress are the two competing mechanisms for fiber buckling.

As the fiber tows are compacted, the resin is squeezed out. The rate of flow due to compaction will depend on the viscosity of the resin. In dry winding, resins of higher viscosity are used, and hence relatively little resin flow occurs during winding itself. However, during curing, the temperature rise causes a drop in the resin viscosity, and the resin can flow easily accompanied by fiber motion until cure sets in.

The stress development during winding has been studied by a number of investigators [1-5]. A comprehensive discussion on the stress development at various stages of filament winding process is given by Tarnapol'skii and Beil' [1]. One of the difficulties with the stress analysis is that the effective stress-strain behavior in the radial direction is nonlinear. Tarnapol'skii and Beil' [1] presented results based on linear, piecewise linear and nonlinear elastic analyses. Cai et al. [4] used a piecewise linear elastic analysis while Lee, Springer, et al. [2, 3] as well as Spencer [5] used a linear elastic analysis based on an effective radial modulus. Since these investigators except [1] were interested in modeling the whole filament winding process, no experimental correlation was provided for the stresses due to winding only.

Recently, Hahn and Lee [6] investigated the stress development during winding of dry glass fibers on a circular mandrel of 58-mm diameter. The wound composite cylinders were about 25 mm thick containing more than 100 layers. They used a linear elastic analysis and found an effective radial modulus by fitting the prediction to the experimentally measured pressure at the mandrel surface. The ratio of the hoop modulus to the inferred radial modulus was in the order of 10^4, indicating a much higher anisotropy than discussed by Tarnapol'skii and Beil' [1]. From the theory-experiment correlation they concluded that the axial fiber stress was compressive, although small in magnitude, throughout most of the cylinder thickness [6]. The compressive nature of the fiber stress was also pointed out in [1].

While the small elastic compressive stresses resulting from winding are unlikely to cause fiber buckling, any fiber motion through the viscous resin may change the state of stress further to favor fiber buckling. The change of stress resulting from fiber motion has been studied by the same investigators mentioned earlier [2-5]. In all cases, the Darcy's law was used in one form or another to represent the resin flow.

The present paper describes an analysis to determine the effect of fiber motion on the stress redistribution in a filament-wound cylinder. Unlike the previous approaches, the radial strain due to fiber motion is represented by a radial creep strain. Thus the present approach is more appropriate when the fiber motion is the result of the slack in the wound cylinder rather than of the fibers moving

through a liquid resin. The main objective is to determine whether or not the radial creep will lead to increased compression of fibers in thick cylinders. Because winding tension is the main parameter controlled during filament winding, simulations are performed to understand how winding tension will affect the stress development during winding and curing.

2. ANALYSIS

Consider a filament-wound cylinder which has just been wound. During winding, stress relaxation is assumed to be negligible. As the cylinder waits for curing, however, fibers start to move radially. The fiber movement can also be during curing. In any case, the severity of fiber movement will depend on the resin viscosity and the amount of slack in the wound cylinder. The objective here is to find the stress redistribution resulting from such fiber movement.

A linear elastic winding analysis is described in detail in [6]. The stresses due to winding are obtained from a plane-stress solution for a cylindrically orthotropic ring. The stress field and fiber positions calculated from the winding analysis are the initial conditions for the stress relaxation analysis resulting from fiber motion.

The initial radial and hoop stresses induced by winding are denoted σ_r^o and σ_θ^o, respectively. The total stresses in the cylinder are then given by

$$\sigma_r^T = \sigma_r^o + \sigma_r \tag{1}$$

$$\sigma_\theta^T = \sigma_\theta^o + \sigma_\theta \tag{2}$$

where σ_r and σ_θ are the additional stresses resulting from fiber movement. When there is a slack and the resin viscosity is low, fibers will move into positions to reduce the radial stress as much as possible. The resulting radial strain is a creep strain and is denoted by ε_r^c. Furthermore, the creep strain rate is assumed to be proportional to the total radial stress:

$$\frac{\partial \varepsilon_r^c}{\partial t} = K\sigma_r^T \tag{3}$$

In the present analysis, K is assumed to be a constant. However, in reality, it would depend on the fiber volume fraction.

The stresses induced by the radial creep satisfy the equilibrium equation

$$\frac{\partial \sigma_r}{\partial r} + \frac{\sigma_r - \sigma_\theta}{r} = 0 \tag{4}$$

The stress-strain relations are given by

$$\varepsilon_r - \varepsilon_r^c = \frac{\sigma_r}{E_r} - v_{r\theta}\frac{\sigma_\theta}{E_\theta} \tag{5}$$

$$\varepsilon_\theta = \frac{\sigma_\theta}{E_\theta} - v_{\theta r}\frac{\sigma_r}{E_r} \tag{6}$$

and the strain-displacement relations by

$$\varepsilon_r = \frac{\partial u}{\partial r} \tag{7}$$

$$\varepsilon_\theta = \frac{u}{r} \tag{8}$$

Substituting Eqs. (3)-(8) into Eq. (4) results in the following equation for u:

$$\frac{\partial^2 u}{\partial r^2} + \frac{1}{r}\frac{\partial u}{\partial r} - \frac{1}{r^2}\frac{E_\theta}{E_r}u = \frac{\partial \varepsilon_r^c}{\partial r} - \frac{1}{r}\varepsilon_r^c(v_{\theta r}\frac{E_\theta}{E_r}+1) \tag{9}$$

The other equation required for ε_r^c is found by substituting Eqs. (2), (5) and (6) into Eq. (3):

$$\frac{\partial \varepsilon_r^c}{\partial t} + \frac{KE_r}{1-v_{\theta r}v_{r\theta}}\varepsilon_r^c = K(\sigma_r^0 + \frac{E_r}{1-v_{\theta r}v_{r\theta}}(\frac{\partial u}{\partial r} + v_{r\theta}\frac{u}{r})) \tag{10}$$

The mandrel is assumed to be much stiffer than the composite cylinder, so that the radial displacement of the composite cylinder vanishes at its inner boundary. The radial stress at the outer boundary is zero as no external pressure is applied. With these boundary conditions, the above equations can be solved. Since the initial stresses, σ_r^0 and σ_θ^0, are known at discrete points within the wound cylinder, the partial differential equations will be solved numerically.

Numerical solution of the partial differential equations is obtained by iterating between an explicit finite difference equation for creep strain and an implicit finite difference equation for the radial displacement [7]. The explicit finite difference form of Eq. (10) is given by

$$\frac{\varepsilon_{j+1,k}^c - \varepsilon_{j,k}^c}{\Delta t} + KA\,\varepsilon_{j,k}^c = K\sigma_r^0 + KA(\frac{u_{j+1,k+1} - u_{j+1,k}}{\Delta r} + \frac{v_{r\theta}}{r_k}u_{j,k}) \tag{11}$$

where $A = \dfrac{E_r}{1 - v_{\theta r} v_{r\theta}}$, and j and k denote the previous time and radius steps, respectively. On the other hand, Eq. (9) is changed into an implicit finite difference equation

$$\frac{u_{j+1,k+1} - 2u_{j+1,k} + u_{j+1,k-1}}{(\Delta r)^2} + \frac{1}{r_k} \frac{u_{j+1,k+1} - u_{j+1,k-1}}{2\Delta r} - \frac{B}{r_k^2} u_{j+1,k}$$

$$= \frac{\varepsilon^c_{j+1,k+1} - \varepsilon^c_{j+1,k-1}}{2\Delta r} - \frac{1}{r_k} C \varepsilon^c_{j+1,k-1} \tag{12}$$

where $B = \dfrac{E_\theta}{E_r}$ and $C = v_{\theta r} B + 1$.

Since $u_{j-1,k}$ is not known *a priori*, $u_{j-1,k}$ is taken to be equal to $u_{j,k}$ for the first iteration. Applying the initial conditions, $u_{0,k} = \varepsilon^c_{0,k} = 0$, $\varepsilon^c_{1,k}$ can be solved at all k increments. With $\varepsilon_{j-1,k}$ known from Eq.

(11) and applying the boundary conditions, $u_{j,0} = 0$ and $\dfrac{u_{j,n} - u_{j-1,n}}{\Delta r} = 0$ where n is the total number of layers, $u_{j-1,k}$ can be determined for all k by solving the k simultaneous equations in Eq. (12). The new value for $u_{j-1,k}$ is then used in Eq. (11) to recalculate $\varepsilon_{j-1,k}$. The iterative process continues until there is no appreciable difference between iterations.

3. RESULTS AND DISCUSSION

A computer program was written to calculate stresses and strains resulting from stress relaxation after winding using the finite difference formulation described in the preceding section. The initial stress state in the cylinder was calculated using the linear elastic winding analysis detailed in [1].

Simulations were performed to calculate the stress development during winding and the subsequent stress relaxation for winding tensions varying between 11.0 N and 44.5 N. The input properties used are listed in Table 1. These properties were inferred from the results of Reference [1].

The creep constant, K, was estimated using data from consolidation experiments included in [6]. Pressure sensors located on the mandrel surface were used to measure the variation in mandrel pressure during consolidation of a cylindrical part. Test results showed a large pressure decrease

with time which gradually approached a constant value after about 60 minutes. The length of time required for relaxation of the mandrel pressure was considered in choosing a value for K. A value of $6.9 \times 10^{-9} (MPa \cdot sec)^{-1}$ was found to cause a similar response as that shown in [6].

The predicted mandrel pressure as a function of time is shown in Fig. 1 for four winding tensions. While the initial pressures due to winding range from 0.3 MPa to 1.4 MPa, they decrease exponentially with time and all converge close to 0.1 MPa after about 60 minutes of relaxation. Therefore, regardless of winding tension, the time required for complete stress relaxation is approximately the same. Also, because mandrel pressure can be conveniently measured by placing pressure sensors at the mandrel-composite interface, experimental determination of the creep constant can be obtained by correlation with the predicted mandrel pressure for a specific cylinder.

Figure 2 shows the initial and final radial stress distributions for a cylinders wound with 11.0 N and 44.5 N winding tensions. While, initially, the radial stresses are much higher for the higher winding tension, after relaxation, radial stresses drop below 0.05 MPa throughout both cylinders. Therefore, fiber support due to the radial stresses will be no greater for cylinders wound with large winding tensions. This is an important result because compressive circumferential stresses after winding were found to be larger for cylinders wound with high winding tensions.

The circumferential stress distribution at several times during relaxation is shown in Fig. 3. Initially, the circumferential stress is slightly compressive through most of the cylinder. As stress relaxation occurs, the magnitude of circumferential stress increases with the greatest increase occurring at the outer layer. Figure 4 shows the change in the maximum compressive stress versus time for each winding tension. A large increase in the circumferential compressive stresses is seen to occur due to stress relaxation. For the lowest winding tension, 11.0 N, the maximum compressive stress increases by a factor of 5.7, while for the highest winding tension, 44.5 N, the maximum compressive stresses increases by a factor of 5.1. Therefore, while compressive stresses are generally larger in cylinders wound with higher tension, the increase due to stress stress relaxation is slightly greater in cylinders wound with lower tension. Changes in the fiber volume fraction resulting from the stress relaxation are shown in Fig. 5. Aside from the region near the outer boundary, the fiber volume fraction changes very little.

The predicted change in the state of stress due to fiber movement favors fiber buckling. The compressive axial fiber stress increases while the compressive radial stress decreases. Since the latter prevents fibers from buckling, the probability of fiber buckling increases during stress relaxation.

4. CONCLUSIONS

In the present study, a model was developed to predict the stress redistribution caused by stress relaxation after winding. The relaxation may occur during the waiting period before curing or during curing itself. The stress relaxation was effectively accounted for by using a creep constant in the

radial direction. Simulations were performed for thick cylinders wound with glass fibers. Winding tension was varied from 11.0 N to 44.5 N.

Although the axial compression on fibers was rather small right after winding, it can increase substantially during stress relaxation. In fact, simulations indicate that the axial compression can increase by as much as a factor of five. Furthermore, the compressive radial stress, which provides lateral support for the fibers, decreases in magnitude. Also, while the initial radial stresses were highest for the winding tension of 44.5 N, the final radial stress distribution decreased to about 0.5 MPa for all winding tensions. The net result is a heightened probability of fiber buckling during stress relaxation.

Acknowledgments

References

1. Tarnopol'skii, Y.M. and Beil', A.I., " Problems of the Mechanics of Composite Winding." Chapter II in *Handbook of Composites, Vol. 4: Fabrication of Composites*, A. Kelly and S.T. Mileiko, Eds., Elsevier Science Publisher B.V., 1983, p.45.

2 Lee, S.Y. and Springer, G.S., "Filament Winding Cylinders: I. Process Model." *Journal of Composite Materials*, Vol. 24, 1990, p. 1270.

3. Calius, E.P., Lee, S.Y. and Springer, G.S., "Filament Winding Cylinders: II. Validation of the Process Model," *Journal of Composite Materials*, Vol. 24, 1990, p. 1299.

4. Cai, Z., Gutowski, T.G., and Allen. S., "Winding and Consolidation Analysis for Cylindrical Composite Structures," *Journal of Composite Materials*, Vol. 26, 1992, p. 1374.

5. Spencer, B.E., "Prediction of Manufacturing Stresses in Thick-Walled Orthotropic Cylinders." Ph.D. thesis, 1988, The University of Nebraska-Lincoln.

6. Hahn, H.T. and Lee, S.S., "The Stress Development During Filament Winding of Thick Cylinders", ONR Report, 1992.

7. Carnahan, B., Luther, H.A., and Wilkes, J.O., *Applied Numerical Methods*. John Wiley and Sons. Inc., 1969, p. 429.

Table 1. Input properties

<u>Composite</u>

Property	Winding Tension, N			
	11.00	22.25	33.50	44.50
E_θ, GPa	36.24	36.24	36.24	36.24
$v_{\theta r}$	0.22	0.22	0.22	0.22
E_r, MPa	4.31	5.17	6.03	6.89
V_f	0.50	0.50	0.50	0.50
Layer Thickness, μm	224	224	224	224
Number of Layers	100	100	100	100

<u>Mandrel</u>

$E_m = 68.95\ GPa,$ $v_m = 0.33,$ inner radius = 25.4 mm,   outer radius = 28.8 mm
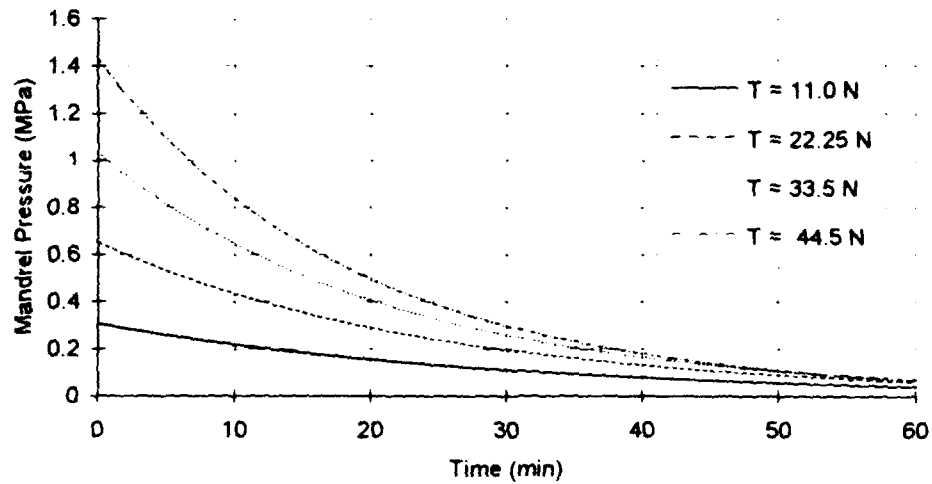
Figure 1. Change in mandrel pressure with time
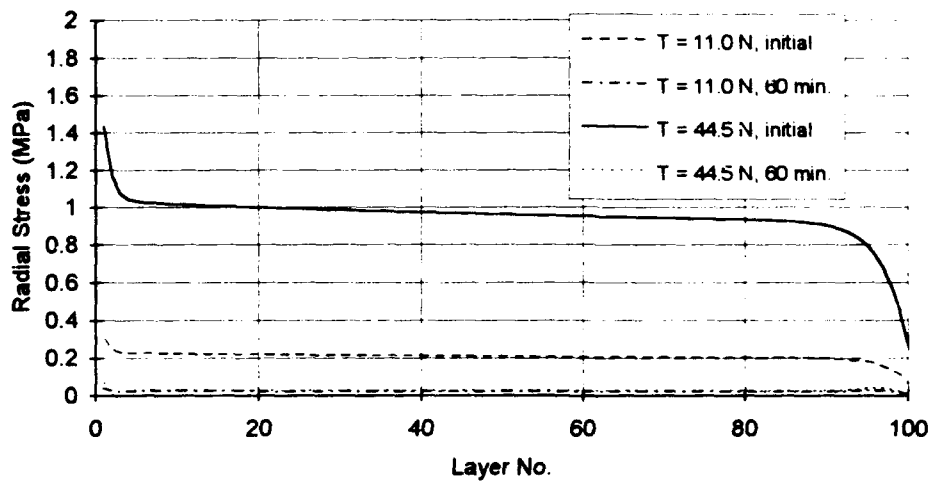
Figure 2. Initial and final radial stress distributions, T = 11.0 N and T = 44.5 N
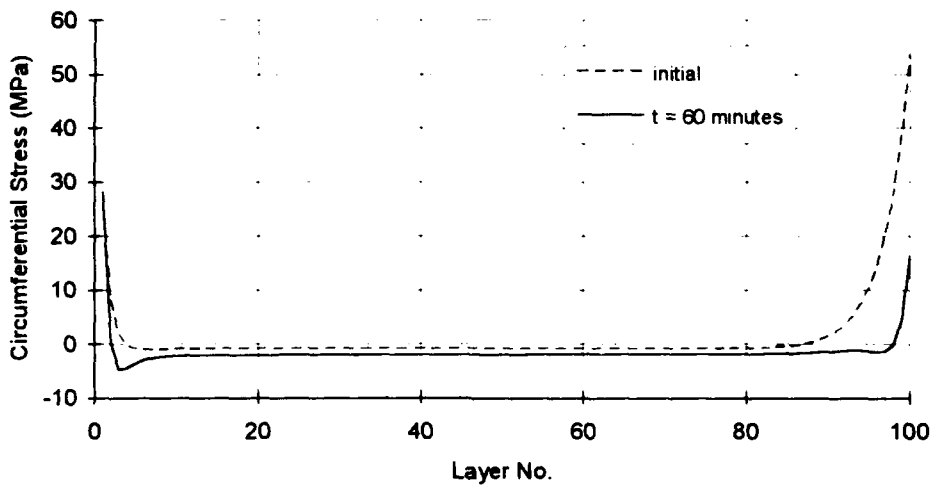
Figure 3. Initial and final circumferential stress distributions, T = 44.5 N
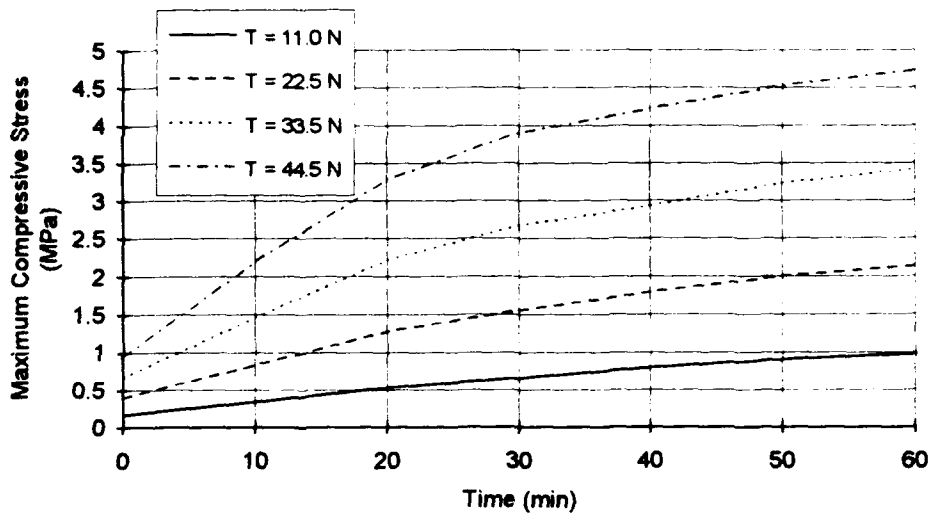
Figure 4. Change in maximum compressive stress with time
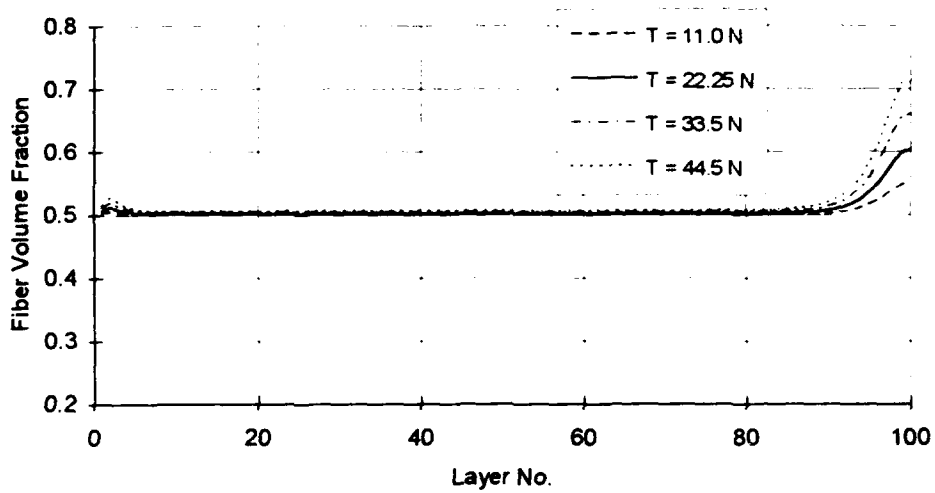
Figure 5. Fiber volume distribution after 60 minutes of stress relaxation